Int. J. Heat Mass Transfer. Vol. 9, pp. 1377–1390. Pergamon Press 1966. Printed in Great Britain

BUBBLE GROWTH RATES AT HIGH JAKOB NUMBERS

ROBERT COLE and HERMAN L. SHULMAN

Department of Chemical Engineering, Clarkson College of Technology, Potsdam, New York

(*Received* 26 *November* 1965 *and in final revised form* 25 *March* 1966)

Abstract—Bubble growth rates were investigated experimentally to determine the effect of high Jakob number conditions. Comparison of the experimental data with existing theory for Jakob numbers ranging from 24 through 792 indicates that the shape of the bubble growth curve over the entire range investigated is best described by the $t^{\frac{1}{2}}$ variation predicted by the uniform superheat model.

Reasonable agreement with the magnitude of the bubble growth data was obtained only for Jakob numbers less than 100. Above this value, the discrepancy between existing theory and experiment becomes increasingly greater. At a Jakob number of 792, theory predicts bubble diameters almost an order of magnitude greater than those found experimentally.

The growth data over the entire range of Jakob numbers investigated were correlated by the expression

$$D = 5\,N_{Ja}^{\frac{1}{2}}\sqrt{(\alpha t)}.$$

It is apparent however that serious shortcomings exist in current bubble growth theory and it is recommended that the theory be re-examined to determine the relative importance of dynamic effects, particularly at high Jakob numbers.

NOMENCLATURE

A, Exposed surface area of ribbon [L];
a, maximum bubble length [L];
b, maximum bubble width [L];
C, specific heat at constant pressure $[HM^{-1}T^{-1}]$;
c, see equation (1); equal to B [L];
D, bubble diameter, defined by equation (2) [L];
E, voltage drop [V];
I, line current [A];
k, thermal conductivity $[H\Theta^{-1}L^{-1}T^{-1}]$;
l', thickness of thermal boundary layer at end of waiting period; see equation (17) [L];
L, ribbon length [L];
N_{Ja}, Jakob number $= \Delta T C_1 \rho_1/\rho_v \lambda$ [dimensionless];
n, integer, equation (14);
P, pressure [mm Hg];
q, heat flux $[H\Theta^{-1}L^{-2}]$;
r, radial distance [L];
R^*, critical bubble radius [L];
t, time [Θ];
t', ribbon thickness [L];
T, temperature [T];
T_0, bulk liquid temperature [T];
T_v, saturation temperature of vapor [T];
T_w, wall temperature. Assumed equal to volume average ribbon temperature [T];
T_s, saturation temperature of liquid at system pressure [T];
ΔT, temperature difference [T];
w, ribbon width [L].

Greek symbols

α, thermal diffusivity $[L^2\Theta^{-1}]$;
β, growth constant, defined by equation (10) [dimensionless];
δ, thermal boundary-layer thickness [L];
λ, latent heat of vaporization $[HM^{-1}]$;
ρ, density $[ML^{-3}]$;
ρ', electrical resistivity [$\mu\Omega$ in];
ϕ_v, ϕ_s, ϕ_b, volume, surface, and base factors for equation (16): defined in reference [6] [dimensionless];

ϕ_c, sphericity correction factor [dimensionless].

Subscripts

b, bubble;
l, liquid;
s, sphere;
v, vapor;
w, wall.

INTRODUCTION

BUBBLE growth rates have been investigated quite extensively for fluids such as water and methanol boiling from solid surfaces under conditions of atmospheric pressure or greater corresponding to Jakob numbers less than 50 [1–6, etc.]. Little attention has been paid to growth rates at sub-atmospheric pressure conditions however, possibly as a result of the analyses of Birkhoff *et al.* [7] and Scriven [8] who for the situation of asymptotic bubble growth in a uniform superheated fluid of infinite extent, showed that the analysis of Plesset and Zwick [9] was a good approximation for values of the dimensionless Jakob number much greater than unity. The Jakob number for water boiling at 50 mm Hg pressure with a superheat of 37 degF is 792, thus meeting this condition. Griffith [10] however, in one of the first analyses attempting to account for the effect of the heating surface, stated that "the range covered by the computer results was limited by the validity of the mathematical model. For very large values of the parameter C (Jakob number) the assumption that the dynamic effects are unimportant is not valid."

The objective of this work was to determine whether bubble growth theories advanced to date (all of which neglect dynamic or inertial effects as being unimportant after the first few microseconds) reasonably describe growth rates from solid surfaces at high Jakob numbers.

EXPERIMENTAL APPARATUS AND PROCEDURE

The system, illustrated schematically in Fig. 1 consisted of an insulated aluminum tank fitted with 4-in diameter by $\frac{3}{8}$-in thick Pyrex glass windows in the front, back and top for purposes of viewing and illumination. The test section from which boiling occurred was suspended horizontally within the tank by

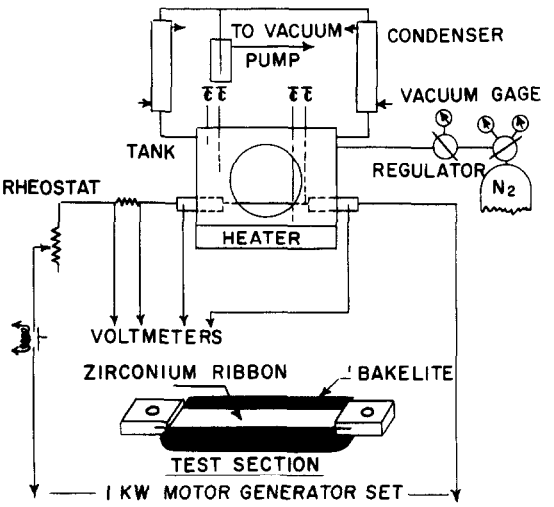

FIG. 1. Schematic diagram of apparatus.

means of $\frac{3}{4}$-in dia. copper bus-bars extending through the tank walls at each end, and which were insulated from the tank itself by means of O-seal straight thread connectors machined from Teflon.

The test section consisted of a polished zirconium ribbon ($\frac{1}{2} \times 4 \times 0{\cdot}01$ in) silver soldered to copper terminals at each end, and cemented to the flat side of a length-wise sliced 1-in diameter Bakelite rod. The cement employed was Ray-Bond R-86004, a thermo-setting type synthetic resin which is unaffected by most organic solvents and which will maintain its adhesive strength to 300°F. The cementing and polishing procedure resulted in a highly polished flush surface on which no edge bubbles formed during operation until ribbon temperatures were reached where thermal expansion effects caused the ribbon to break away from its cement and Bakelite backing.

The test section was bolted to the copper bus-bars in the tank by means of the copper terminals at each end.

Sub-atmospheric pressures were obtained by means of a vacuum pump, protected from the organic vapors by means of an absorbent filled absorption trap in series with an acetone–dry ice cold trap. Pressure regulation was provided by bleeding extra dry nitrogen into the system through a combination vacuum regulator and vacuum gage.

In order to maintain constant liquid level over the period of operation (normally 6–8 hr), the vapors were condensed externally and refluxed to the tank. The liquid in the tank was heated to its saturation temperature and maintained at that level by a thermostatically controlled electric heater in direct contact with the uninsulated bottom of the aluminum tank. To minimize convection currents in the region of the test section, a 5 × 4-in glass plate with ceramic legs was placed $\frac{1}{2}$-in below the surface of the zirconium ribbon.

The zirconium ribbon was heated electrically by means of direct current originating in a 1 kW motor-generator set and the power level to the ribbon controlled by 3 air-cooled 1 kW rheostats connected in parallel. The power input to the ribbon was measured by a voltmeter accurate to $\pm 0{\cdot}5$ per cent attached across the copper bus-bars leading into the tank and a millivoltmeter accurate to ± 1 per cent attached across one of several calibrated resistances in series with the ribbon. The volume average ribbon temperature was obtained for each run by calibration of the zirconium ribbon as a resistance thermometer.

Liquid and vapor temperatures were measured by means of 4 copper–constantan thermocouples extending through the top of the tank. The vapor temperature was measured at one of the two vapor exits, and the liquid temperature was measured at a point close to the liquid surface, at the level of the zirconium ribbon, and at a point close to the bottom of the tank.

The boiling action on the ribbon was recorded by means of an 8-mm "Fastax" camera equipped with a 50 mm f/2 lens and capable of operating at speeds to 16000 frames per s. The actual operating speed was determined by the frequency of bubble formation on the ribbon. At the lower pressures where extremely low bubble frequencies were observed, the camera was operated at 3000 frames per s. At pressures near atmospheric, a 10000 frames per s camera speed was employed. Close-up pictures for the small bubbles observed near atmospheric pressure were obtained by the use of extension tubes. Lighting was provided by means of two 750-W reflector lamps located behind the tank. One thousand or 100 c/s timing marks depending on the film speed were recorded on the film by means of a timing light generator and a neon timing lamp within the camera.

In order to scale the images to actual size, a wire of known diameter was suspended just above the center of the ribbon and toward one end. The wire appeared in each frame of the film and because few bubbles formed near the ends of the ribbon, it did not affect the bubble action and had the additional advantage of providing an object on which to focus the camera which was known to be in the same plane as the vapor bubbles.

Liquids and pressures for which data were obtained include toluene at 48 mm Hg, acetone at 222 mm Hg, *n*-pentane at 524 and 760 mm Hg, carbon tetrachloride at 138 mm Hg, methanol at 5 pressures ranging from 134 to 540 mm Hg, and water at 4 pressures from 50 to 360 mm Hg. In all cases, heat flux values were less than 15 per cent of the critical heat flux.

METHODS OF MEASUREMENT AND CALCULATION

In order to obtain quantitative information on the dynamics of the bubble motion, the film was analyzed frame by frame using a Vanguard Motion Analyzer which supplied a 15× magnification of film size to viewed image.

Tracings of acetone bubble number 3 as a

function of time are illustrated in Fig. 2. It is to be noted from Fig. 2 that the zero time has been defined as the first frame prior to the bubble being observed. Thus an error is unavoidably introduced into the time measurements which may have a maximum value equal to the time between successive frames. For acetone bubble number 3, the maximum error is $-0{\cdot}25$ ms since the film speed at nucleation was 4000 frames per s.

In this work, visual observation of the bubble growth through the top of the boiling tank indicated that spreading would occur along the length of the ribbon rather than along its width. To take this into account, the bubbles were assumed to be ellipsoidal in shape with the longest axis along the ribbon length and the unknown axis equal to the vertical axis of the ellipsoid. The assumed shape is illustrated in Fig. 3 and should be compared to the tracings shown in Fig. 2.

The volume of the ellipsoid is given by

$$V_b = \frac{\pi}{6} abc \quad = \frac{\pi}{6} ab^2. \tag{1}$$

Bubble diameters are here defined as the diameter of a sphere having the same volume as a bubble.

$$D_s = \left(\frac{6}{\pi} V_b\right)^{\frac{1}{3}}. \tag{2}$$

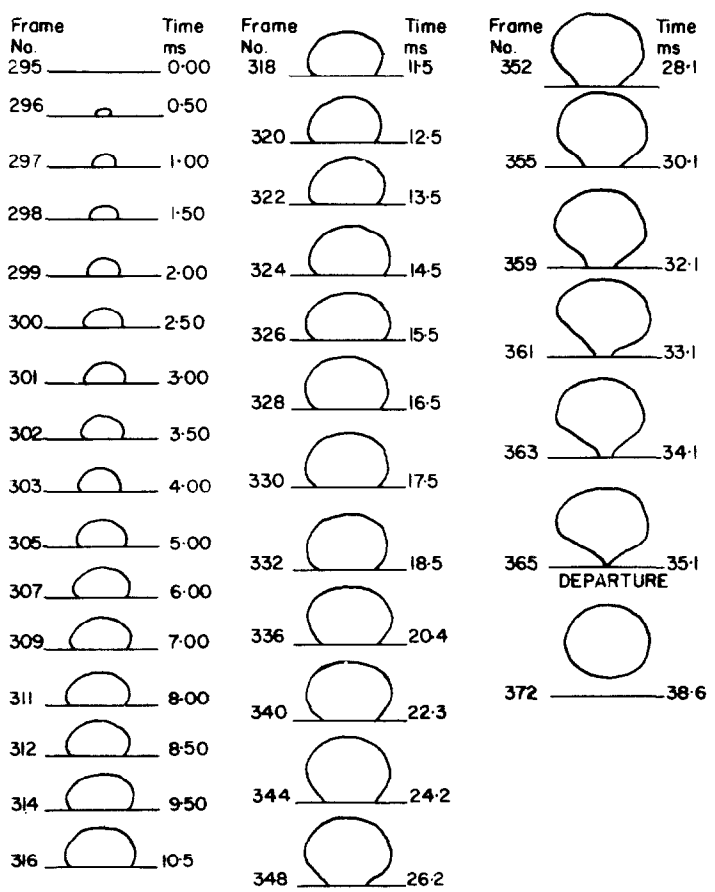

FIG. 2. Bubble growth tracings for acetone bubble number 3.

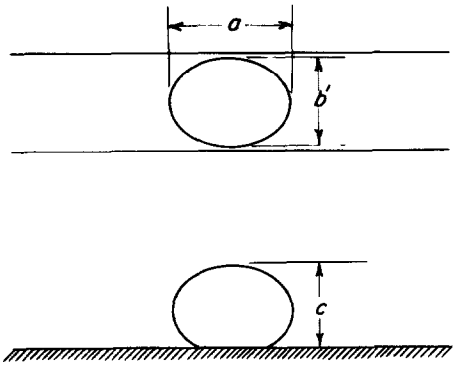

FIG. 3. Assumed bubble shape.

Substituting equation (1) into equation (2), the bubble diameter is given as

$$D_s = (ab^2)^{\frac{1}{3}}. \quad (3)$$

Using equation (3) to compute bubble diameters from the data obtained from the film, bubble growth curves were plotted for each of the 92 bubbles investigated.

Other sources have not been quite as elaborate in defining the equivalent diameters of their bubbles. For example, Han and Griffith [6] define the bubble diameter as the geometric mean of the bubble diameters in the two principal axis directions. Thus

$$D_s = (ab)^{\frac{1}{2}}. \quad (4)$$

Siegel and Keshock [5] define the bubble diameters as the arithmetic mean of the diameters in the two principal axis directions. Thus

$$D_s = \frac{a+b}{2}. \quad (5)$$

Bubble diameters computed from equations (3–5) are plotted in Fig. 4 for comparison. Three distinct growth curves result and the deviation from the mean appears to be of the order of ± 10 per cent. Although this is not necessarily an indication of the actual degree of error involved in the experimental growth curves, it is an indication that the method of determining bubble diameters is not critical.

In addition to the bubble growth curves,

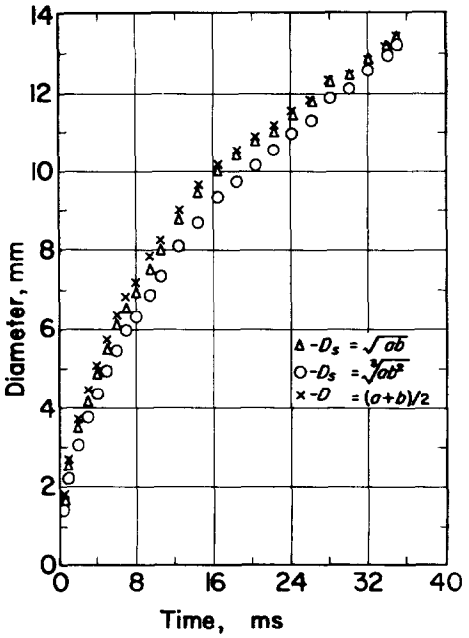

FIG. 4. Comparison of experimental growth curves for acetone bubble number 3 using different diameter expressions.

bubble diameters, velocities and contact angles were determined at departure. This data has been reported elsewhere [11] and hence is not tabulated here.

Heat flux levels were determined from a knowledge of the voltage drop across the ribbon, the line current and the exposed surface area.

$$q = \frac{3{\cdot}414EI}{A}. \quad (6)$$

Assuming all of the heat generated to be transferred through the exposed surface, the estimated maximum error in the heat flux is ± 2 per cent. Analysis [12] indicates that under conditions typical of this work, the heat loss to the copper bus-bars is probably less than 10 per cent of the total heat generation as determined from equation (6).

The volume average ribbon temperature was determined by calibration of the zirconium ribbons as resistance thermometers. A least squares fit of the data for three ribbons having

different lengths, widths, and thicknesses resulted in the following expression for resistivity as a function of temperature from 68 to 400°F.

$$\rho' = 20{\cdot}9[1 + 0{\cdot}00171(T - 68)] \quad (7)$$

where T is in °F and ρ in μΩ in. The standard deviation for this expression was 0·45 μΩ in.

Following the initial calibration, the ribbons were mounted on the Bakelite half-rods and polished. A second calibration was obtained at several temperatures for each ribbon while mounted in place in the boiling tank just prior to an actual run. Comparison of the two calibration curves yielded the new ribbon thickness resulting from the polishing operation.

Under operating conditions the volume average ribbon temperature was determined from voltage and current measurements, the ribbon dimensions and the calibration curve by means of the equation

$$\rho' = \frac{E}{I}\frac{wt'}{L}. \quad (8)$$

The estimated maximum error in the volume average ribbon temperature as determined by this procedure ranges from ±9 to ±13 per cent.

The degree of superheat reported here is the difference between the volume average temperature of the ribbon and the saturation temperature corresponding to the pressure at the ribbon surface. The average maximum error in the superheat is estimated to be ±50 per cent.

RESULTS AND DISCUSSION

The analyses for bubble growth in a uniformly superheated liquid of infinite extent should not be expected to yield agreement with data obtained for growth from a solid surface in a non-uniform temperature field. However, because the resulting expressions are of such simple form [9, 13, 14]

$$D = \phi_c \frac{4}{\pi} N_{Ja} \sqrt{(\pi\alpha t)} \quad (9)$$

it is worthwhile to determine the extent to which they can approximate the data. The most meaningful method for such a comparison results from the analysis of Scriven [8], where

$$D = 4\beta\sqrt{(\alpha t)} \quad (10)$$

and the asymptotic solution for the growth constant β (valid at high Jakob numbers for the uniform superheat conditions of Scrivens analysis) is given by

$$\beta = \frac{\phi_c}{\sqrt{\pi}}\left\{\frac{T_0 - T_v}{\frac{\rho_v}{\rho_1}\left[\frac{\lambda}{C_1} + \left(\frac{C_1 - C_v}{C_1}\right)(T_0 - T_v)\right]}\right\} \cong \frac{\phi_c}{\sqrt{\pi}} N_{Ja}. \quad (11)$$

For the conditions of this work, the term in brackets was approximately equal to the Jakob number. From equation (9), if the diameter is plotted versus $t^{\frac{1}{2}}$, a straight line of slope $4\beta\alpha^{\frac{1}{2}}$ should result, from which the growth constant β can be determined. Equation (10) then relates the growth constant to a modified Jakob number.

When the data obtained in this work were plotted as a function of $t^{\frac{1}{2}}$, in many cases the data were linear, and in most other cases the major portion of the curve could be approximated by a linear relationship. This is of considerable interest as it indicates that the shape of the bubble growth curve over the wide range of Jakob numbers investigated here (24–792) can be adequately represented by the simple $t^{\frac{1}{2}}$ variation predicted by uniform superheat theory.

The growth constants obtained in this fashion are presented graphically in Fig. 5 as a function of modified Jakob number. The data can be compared with equation (9) for values of $\phi_c = 1$, $\pi/2$, and $\sqrt{3}$. Respectively, these represent the expressions of Fritz and Ende [13], Forster and Zuber [14] and Plesset and Zwick [9]. As might be expected, the growth constants predicted from uniform superheat theory are greater than those obtained experimentally for growth from a solid surface in a non-uniform temperature field. Note, however, that the discrepancy is in the magnitude of the growth

constant, and not the shape of the growth curve.

In computing the modified Jakob number, the usual procedure of substituting the wall superheat $T_w - T_s$ for the liquid superheat $T_0 - T_v$ has been followed. This might be a good approximation if the thermal layer in which the bubbles grow was uniformly superheated to the temperature at the wall. Actually, since the liquid superheat approaches zero away from the wall, an average driving force of $\frac{1}{2}(T_w - T_s)$ might be a better approximation. Indeed, as seen in Fig. 5, if the modified Jakob numbers for the data are multiplied by a factor of $\frac{1}{2}$, the results for Jakob numbers less than 100 are in good agreement with theory. Thus for $\phi_c = \pi/2$

$$D = N_{Ja}\sqrt{(\pi\alpha t)}. \qquad (12)$$

Conversely, for Jakob numbers greater than 100, the discrepancy between theoretical and experimental growth constants becomes increasingly greater.

The actual growth data for the bubbles analyzed in this work are shown graphically in Figs. 6–26. It should be noted that most of the figures indicate a large variation in bubble growth rate for apparently identical conditions such as surface heat flux and wall superheat. In fact, however, these conditions are only average values and no account has been made of local conditions such as site dimension and thermal-layer thickness. Had these local factors been determined, the growth rate would still be expected to vary in some statistical fashion since according to Hsu [4] the thickness and

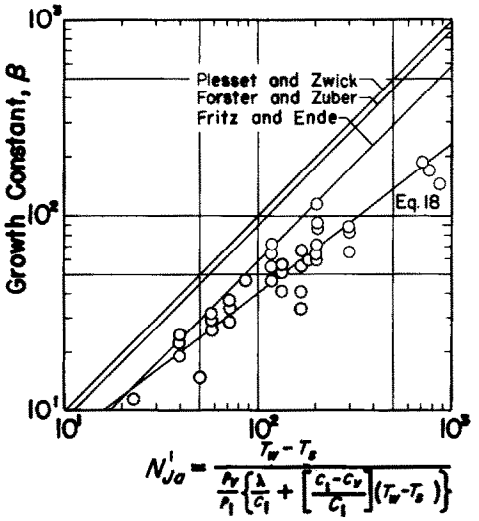

FIG. 5. Comparison of uniform models with data.

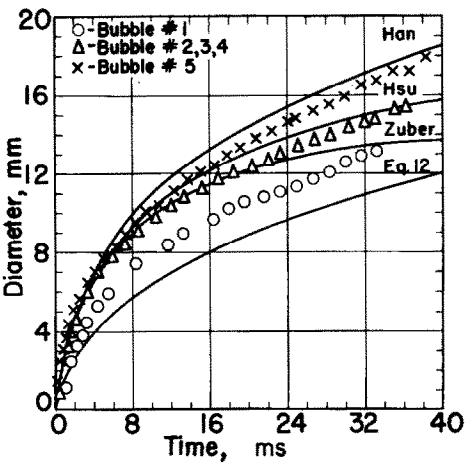

FIG. 6. Bubble growth data for water, $P = 360$ mm Hg, $T_w - T_s = 27$ degF, $N_{Ja} = 87{\cdot}7$, $q = 1{\cdot}99 \times 10^4$ Btu/h ft^2.

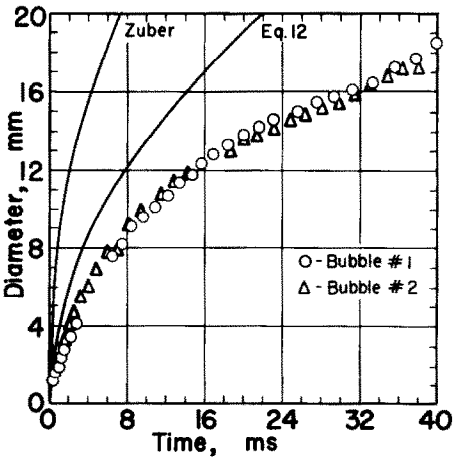

FIG. 7. Bubble growth data for water, $P = 195$ mm Hg, $T_w - T_s = 33$ degF, $N_{Ja} = 191$, $q = 1{\cdot}515 \times 10^4$ Btu/h ft^2.

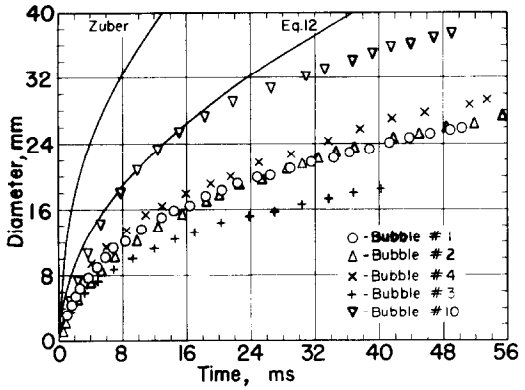

FIG. 8. Bubble growth data for water, $P = 98$ mm Hg, $T_w - T_s = 27$ degF, $N_{Ja} = 301$, $q = 1{\cdot}185 \times 10^4$ Btu/h ft^2.

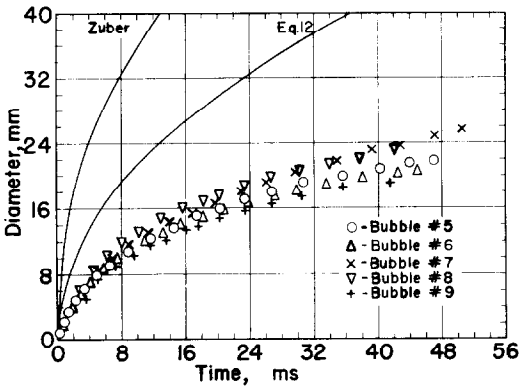

FIG. 9. Same as Fig. 8.

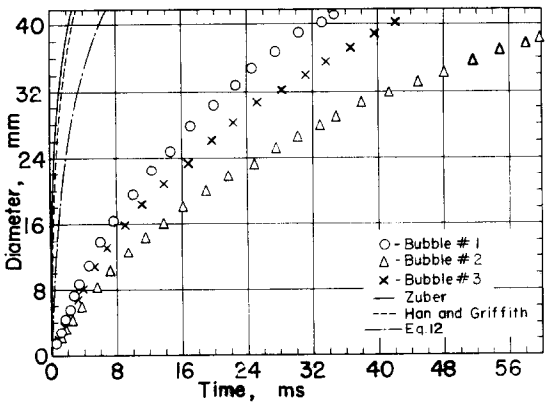

FIG. 10. Bubble growth data for water, $P = 50$ mm Hg, $T_w - T_s = 37$ degF, $N_{Ja} = 792$, $q = 2{\cdot}125 \times 10^4$ Btu/h ft^2.

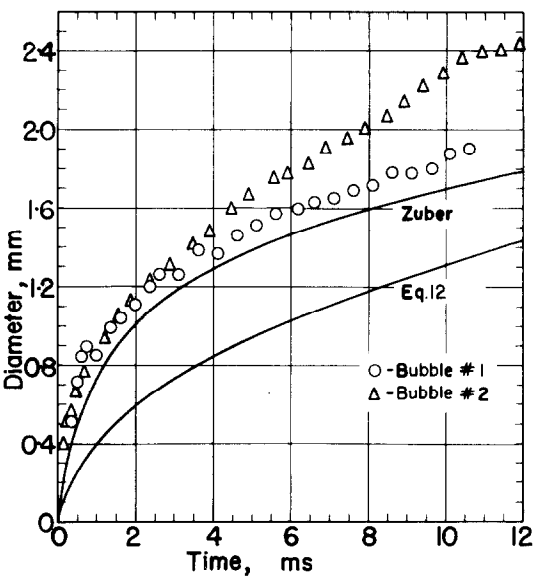

FIG. 11. Bubble growth data for n-pentane, $P = 760$ mm Hg, $T_w - T_s = 31$ degF, $N_{Ja} = 23{\cdot}9$, $q = 0{\cdot}926 \times 10^4$ Btu/h ft^2.

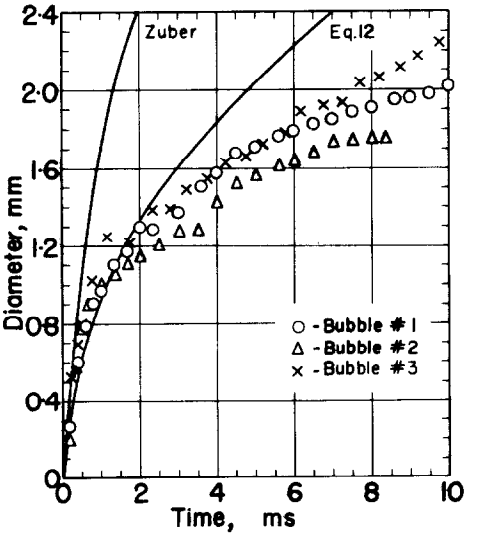

FIG. 12. Bubble growth data for n-pentane, $P = 524$ mm Hg, $T_w - T_s = 50$ degF, $N_{Ja} = 52{\cdot}8$, $q = 1{\cdot}15 \times 10^4$ Btu/h ft^2.

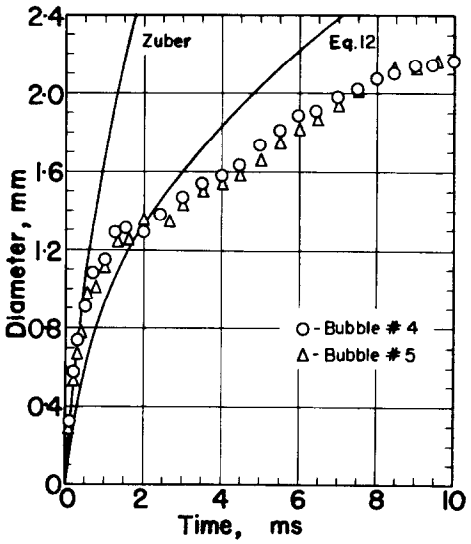

FIG. 13. Same as Fig. 12.

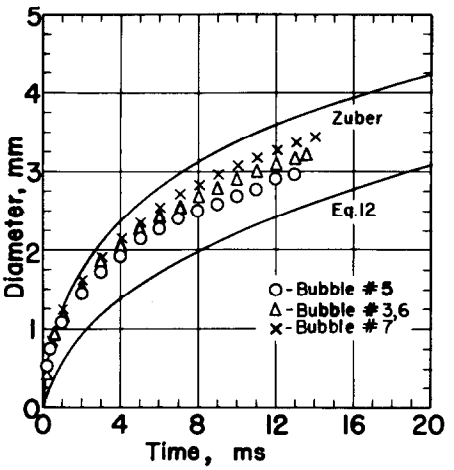

FIG. 15. Same as Fig. 14; $q = 0{\cdot}924 \times 10^4$ Btu/h ft^2.

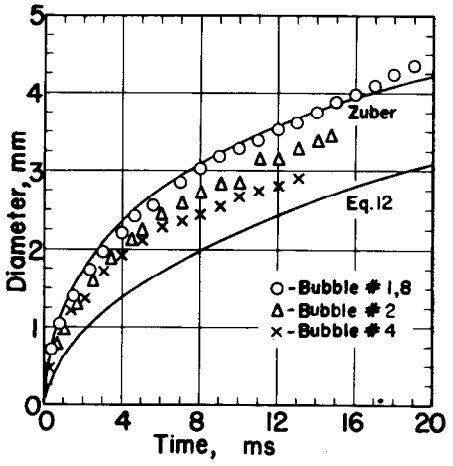

FIG. 14. Bubble growth for methanol, $P = 540$ mm Hg, $T_w - T_s = 32$ degF, $N_{Ja} = 41{\cdot}2$.

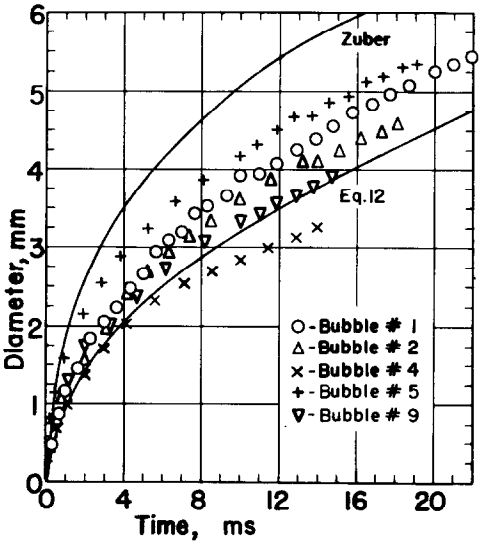

FIG. 16. Bubble growth data for methanol, $P = 397$ mm Hg, $T_w - T_s = 36$ degF, $N_{Ja} = 59{\cdot}6$, $q = 0{\cdot}915 \times 10^4$ Btu/h ft^2.

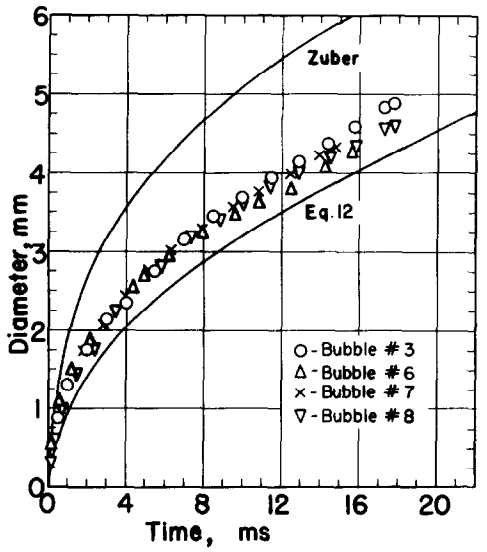

FIG. 17. Same as Fig. 16.

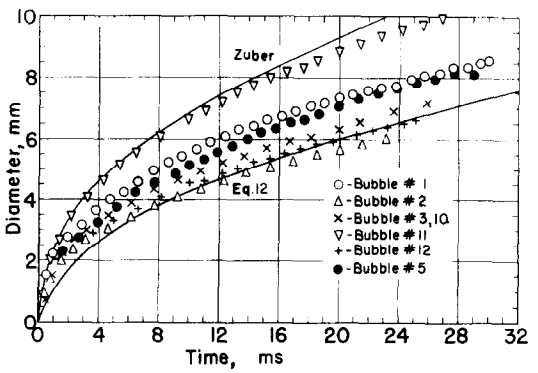

FIG. 18. Bubble growth data for methanol, $P = 304$ mm Hg, $T_w - T_s = 36$ degF, $N_{Ja} = 74{\cdot}6$, $q = 0{\cdot}738 \times 10^4$ Btu/h ft^2.

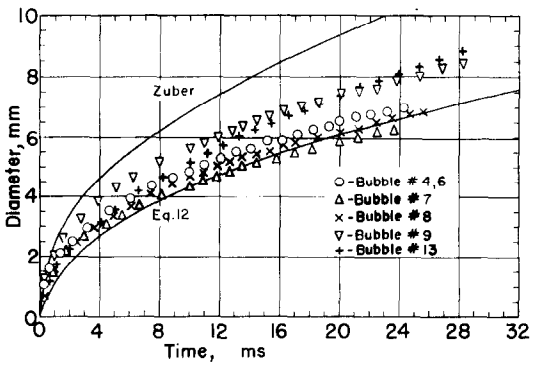

FIG. 19. Same as Fig. 18.

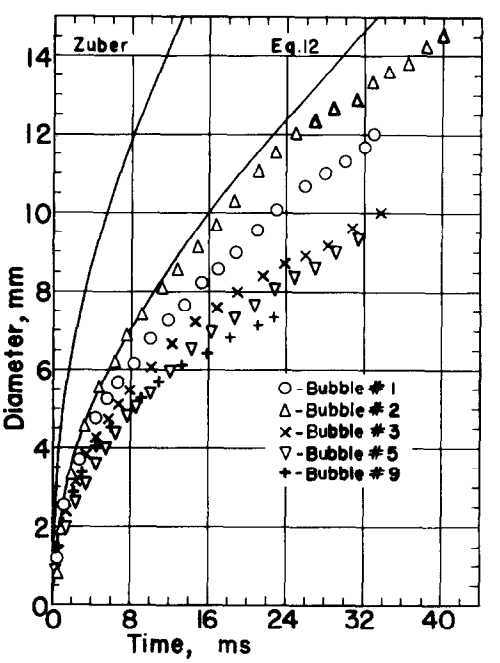

FIG. 20. Bubble growth data for methanol, $P = 204$ mm Hg, $T_w - T_s = 48$ degF, $N_{Ja} = 140{\cdot}5$, $q = 0{\cdot}891 \times 10^4$ Btu/h ft^2.

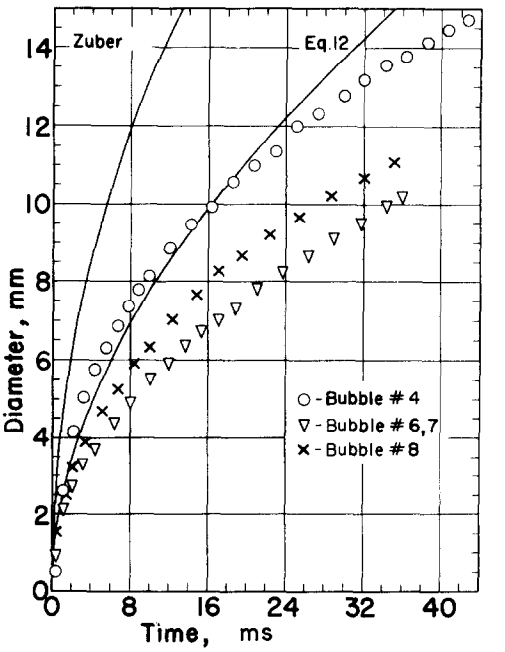

FIG. 21. Same as Fig. 20.

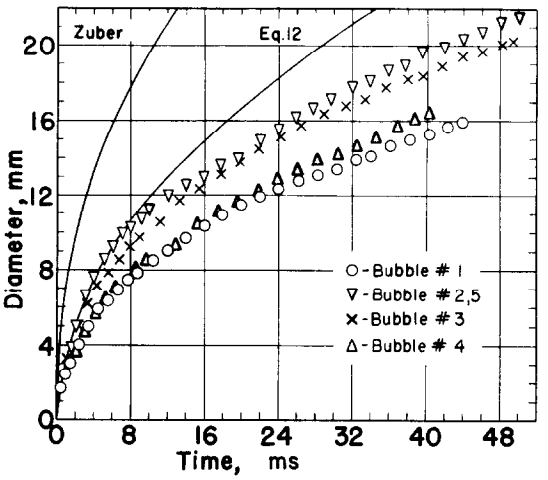

FIG. 22. Bubble growth data for methanol, $P = 134$ mm Hg, $T_w - T_s = 50$ degF, $N_{Ja} = 209$, $q = 1{\cdot}05 \times 10^4$ Btu/h ft^2.

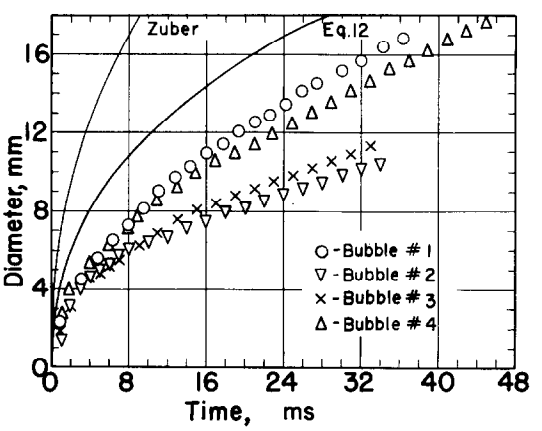

FIG. 23. Bubble growth data for carbon tetrachloride, $P = 138$ mm Hg, $T_w - T_s = 52$ degF, $N_{Ja} = 175{\cdot}5$, $q = 0{\cdot}711 \times 10^4$ Btu/h ft^2.

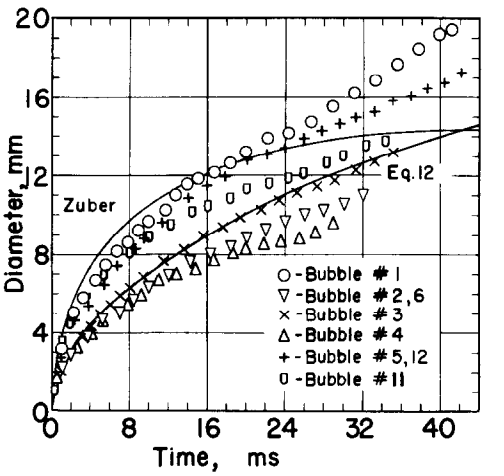

FIG. 24. Bubble growth data for acetone, $P = 222$ mm Hg, $T_w - T_s = 49$ degF, $N_{Ja} = 124$, $q = 1{\cdot}34 \times 10^4$ Btu/h ft^2.

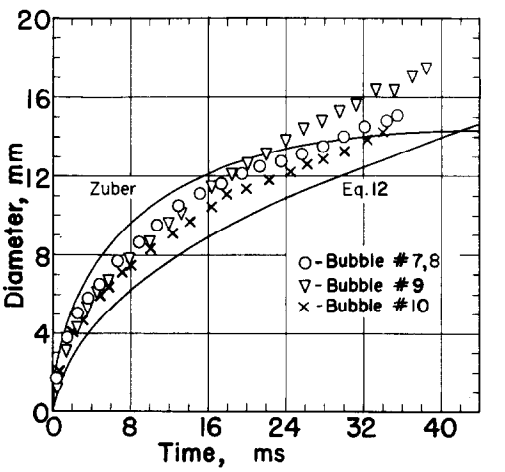

FIG. 25. Same as Fig. 24.

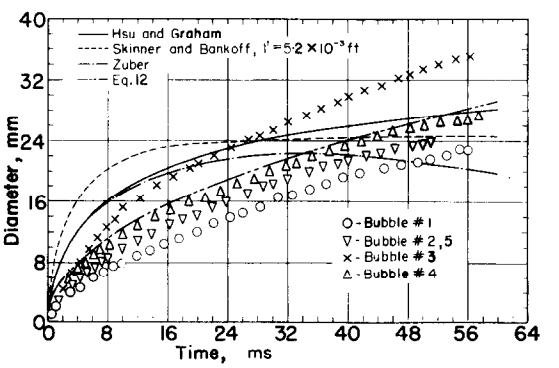

FIG. 26. Bubble growth data for toluene, $P = 48$ mm Hg, $T_w - T_s = 24$ degF, $N_{Ja} = 210$, $q = 0{\cdot}596 \times 10^4$ Btu/h ft^2.

temperature distribution in the thermal layer are influenced by both fluctuating bulk turbulence and past history.

Equation (12) and Zubers expression [15] for bubble growth in a non-uniform temperature field

$$D = \phi_c \frac{4}{\pi} N_{Ja} \sqrt{(\pi \alpha t)} \left[1 - \frac{q_w \sqrt{(\pi \alpha t)}}{2k(T_w - T_s)}\right] \quad (13)$$

with $\phi_c = \pi/2$ are compared with the experimental data in each of the figures.

Hsu and Graham's expression [4] for bubble growth in a non-uniform temperature field

$$D = \frac{\pi}{\lambda \rho_v}\left\{\frac{q_w t}{2\pi} + \frac{2q_w \delta^2}{\alpha \pi^2} \times \left(\frac{\pi^2}{6} \sum_{n=1}^{\infty} \frac{1}{n^2} \exp\left[-\left(\frac{\pi n}{\delta}\right)^2 \alpha t\right]\right)\right\} \quad (14)$$

is compared with the experimental data in Figs. 6 and 26. In employing their equations, since neither delay times nor nucleating site dimensions were measured, the boundary-layer thickness has been expressed as

$$\delta = \frac{k(T_w - T_s)}{q_w}. \quad (15)$$

Thus the resulting expression would be expected to predict only the growth rate of an average bubble. The critical radius was neglected and the second of their two equations used for the entire growth curve with R^* and t^* equal to zero. Furthermore, in this work the bulk temperature of the fluid T_0 was at the saturation temperature and hence the difference in temperature between the vapor in the bubble and the bulk temperature of the liquid has been taken as zero. Calculations indicate that this vapor superheat amounts to only 1 or 2 degF and thus is negligible relative to the wall superheat. Additionally the sphericity factor ϕ_c was chosen as $\pi/2$.

Han and Griffith's expression [6] for bubble growth in a non-uniform temperature field

$$D = \frac{\phi_s \phi_c}{\phi_v} \frac{2k}{\lambda \rho_v} \left\{\frac{2(T_w - T_s)}{\sqrt{(\pi \alpha)}} t^{\frac{1}{2}} - \frac{(T_w - T_0)}{\delta} \frac{\delta^2}{4\alpha} \left(\frac{4\alpha t}{\delta^2} \operatorname{erf} \frac{\delta}{\sqrt{(4\alpha t)}} + \frac{2}{\sqrt{\pi}} \frac{\sqrt{(4\alpha t)}}{\delta} \exp\left[-\frac{\delta^2}{4\alpha t}\right] - \operatorname{erfc} \frac{\delta}{\sqrt{(4\alpha t)}}\right)\right\} \quad (16)$$

is compared with the experimental data in Figs. 6 and 10. Again the critical radius was assumed negligible and the boundary-layer thickness δ determined from equation (15). In Hans equation, no assumption is necessary for the value of ϕ_c as he has expressed this quantity in terms of δ; the contact angle and an average diameter.

The analysis of Skinner and Bankoff [16] for bubble growth in a non-uniform temperature field having an initial temperature distribution given by

$$T(r, b) = T_0 + (T_w - T_0) \exp\left[-\frac{r^6}{9l'^6}\right] \quad (17)$$

is compared with the experimental data in Fig. 26. It is to be noted that there is no *a priori* means of predicting the boundary-layer thickness l' in this analysis as could be done for the previous expressions. For purposes of comparison, an l' was chosen by trial which would yield a final diameter in the range of those found experimentally for toluene in Fig. 26.

The analysis of Bankoff and Mikesell [17] is similar to that of Skinner and Bankoff and also involves an arbitrary constant which is used to fit the analysis to the data. Because of these reasons no comparisons with the experimental data have been made.

The analysis of Griffith [10] has not been compared with this data as the range of Jakob numbers for which solutions were obtained by Griffith are much lower than those in this work. The reason given for not extending the solution to higher Jakob numbers is stated in the introduction and appears to have been justified by the data obtained here.

Comparison of all of the non-uniform temperature field growth equations with the experimental data indicates them to be less satisfactory than the uniform superheat expression given by equation (12). In fact as the equations increase in complexity, they appear to approach the $t^{\frac{1}{2}}$ variation predicted by uniform superheat theory. As with equation (12), reasonable agreement with the magnitude of the growth data is obtained only for Jakob numbers less than 100. Above this value, the discrepancy between theory and experiment becomes increasingly greater.

With the knowledge that equation (12) best represents the data of this work, Fig. 5 can be used to obtain an approximate relationship for the growth constant as a function of Jakob number which when substituted into equation (10) will yield an expression for the bubble growth satisfying both the magnitude and shape of the experimental growth curves. From Fig. 5

$$\beta \cong \tfrac{5}{4}N_{Ja}^{\frac{1}{2}} . \tag{18}$$

Substituting into equation (10)

$$D = 5N_{Ja}^{\frac{1}{2}} \sqrt{(\alpha t)}. \tag{19}$$

Although equation (19) is of some value as it is a simple representation of the data in a region where theory and experiment are in wide disagreement, it is empirical in nature and does not aid in explaining the discrepancies which exist. It seems apparent that the theories for bubble growth from a surface where the temperature field is non-uniform should be re-examined. In particular, emphasis should be placed on determining the relative importance of dynamic effects at high Jakob numbers.

ACKNOWLEDGEMENT

The authors are grateful for the initial support given by the Clarkson College Division of Research and the later support given by The National Science Foundation through Grant Number GP-277.

REFERENCES

1. B. E. Staniszewski, Nucleate boiling bubble growth and departure, *Tech. Rep.* 16, Div. Sponsored Res., MIT, August (1959).
2. M. E. Ellion, A study of the mechanism of boiling heat transfer, *Rept.* 20–88, Jet Prop. Lab., Calif. Inst. Tech. (1954).
3. F. Gunther, Photographic study of surface boiling heat transfer to water with forced convection, *Trans. Am. Soc. Mech. Engrs* **73**, 115 (1951).
4. Y. Y. Hsu and R. W. Graham, An analytical and experimental study of the thermal boundary layer and ebullition cycle in nucleate boiling, *NASA TN D-594*, May (1961).
5. R. Siegel and E. G. Keshock, Effects of reduced gravity on nucleate boiling bubble dynamics in saturated water, *A.I.Ch.E. Jl* **10**, 509 (1964).
6. Chi-Yeh Han and P. Griffith, The mechanism of heat transfer in nucleate pool boiling—Part I, *Int. J. Heat Mass Transfer* **8**, 887 (1965).
7. G. Birkhoff, R. S. Margules and W. A. Horning, Spherical bubble growth, *Physics Fluids* **1**, 201 (1958).
8. L. E. Scriven, On the dynamics of phase growth, *Chem. Engng Sci.* **10**, 1 (1959).
9. M. S. Plesset and S. A. Zwick, The growth of vapor bubbles in superheated liquids, *J. Appl. Phys.* **25**, 493 (1954).
10. P. Griffith, Bubble growth rates in boiling, *Trans. Am. Soc. Mech. Engrs* **80**, 721 (1958).
11. R. Cole and H. L. Shulman, Bubble departure diameters at sub-atmospheric pressures, *Chem. Engng Prog. Symp. Ser., Heat Transfer—Los Angeles* **62** (4), (1966).
12. R. Cole, Bubble dynamics in boiling, Ph.D. thesis, Clarkson College of Technology, Potsdam, New York, October (1965).
13. W. Fritz and W. Ende, Verdampfungsvorgang nach kinematographischen Aufnahmen an Dampfblasen, *Phys. Z.* **37**, 391 (1936).
14. H. K. Forster and N. Zuber, Growth of a vapor bubble in a superheated liquid, *J. Appl. Phys.* **25**, 474 (1954).
15. N. Zuber, The dynamics of vapor bubbles in non-uniform temperature fields, *Int. J. Heat Mass Transfer* **2**, 83 (1961).
16. A. L. Skinner and S. G. Bankoff, Dynamics of vapor bubbles in spherically symmetric temperature fields of general variation, *Physics Fluids* **7**, 1 (1964).
17. S. G. Bankoff and R. D. Mikesell, Growth of bubbles in a liquid of initially non-uniform temperature, *A.S.M.E. paper* 58-*A*-105, A.S.M.E. Annual Meeting, New York (1958).

Résumé—Les vitesses de croissance des bulles ont été étudiées expérimentalement pour déterminer l'effet des nombres de Jakob élevés. La comparaison des résultats expérimentaux avec la théorie actuelle pour des nombres de Jakob compris entre 24 et 792 indique que la forme de la courbe de croissance des bulles dans toute la gamme étudiée est décrite le mieux par la variation en $t^{\frac{1}{2}}$ prédite par le modèle à surchauffe uniforme.

Un accord raisonnable avec la grandeur des résultats de croissance de bulles a été obtenu seulement pour des nombres de Jakob plus petits que 100. Au-dessus de cette valeur, la différence entre la théorie actuelle et l'expérience devient de plus en plus grande. A un nombre de Jakob de 792, la théorie prévoit des diamètres de bulles presque d'un ordre de grandeur au-dessus de ceux trouvés expérimentalement.

La croissance des bulles dans toute la gamme des nombres de Jakob étudiés a été corrélée par l'expression:

$$D = 5N_{Ja}^{\frac{1}{2}}\sqrt{(\alpha t)}.$$

Cependant, il est visible que de sérieuses insuffisances existent dans la théorie ordinaire de la croissance des bulles et il est recommandé que la théorie soit réexaminée pour déterminer l'importance relative des effets dynamiques, particulièrement aux nombres de Jakob élevés.

Zusammenfassung—Wachstumgsgeschwindigkeiten von Blasen wurden experimentell untersucht, um den Einfluss von grossen Jakob-Zahlen zu bestimmen. Ein Vergleich der experimentellen Ergebnisse mit der herkömmlichen Theorie für Jakob-Zahlen zwischen 24 und 792 zeigt, dass die Form der Blasenwachstums-Kurve in dem ganzen untersuchten Bereich am besten durch das $t^{\frac{1}{2}}$-Gesetz wiedergegeben wird, das aus der Vorstellung einer gleichmässigen Überhitzung abgeleitet wird.

Eine gute Übereinstimmung der Blasenwachstumsdaten ergab sich nur für Jakob-Zahlen kleiner als 100. Oberhalb dieses Wertes wird die Diskrepanz zwischen der herkömmlichen Theorie und dem Experiment zunehmend grösser. Bei einer Jakob-Zahl von 792 ergeben sich aus der Theorie Blasendurchmesser, die fast eine Grössenordnung grösser sind als die experimentell gefundenen.

Das Wachstumsgesetz konnte in dem gesamten untersuchten Bereich durch die Gleichung

$$D = 5N_{Ja}^{\frac{1}{2}}\sqrt{(\alpha t)}.$$

dargestellt werden. Es ist offensichtlich, dass die heute gültige Blasenwachstumstheorie bedeutende Mängel aufweist, und es wird vorgeschlagen, diese Theorie zu überprufen, um die Bedeutung von dynamischen Effekten—insbesondere bei hohen Jakob-Zahlen—zu bestimmen.

Аннотация—Сравнение полученных в работе экспериментальных данных по росту пузырьков с существующей теорией для чисел Якоба 24–792 показывает, что рост пузырьков во всем исследованном диапазоне лучше всего описывается зависимостью $t^{\frac{1}{2}}$ для модели однородного перегрева.

Удовлетворительное соответствие с экспериментальными данными по росту пузырьков получено только для чисел Якоба меньше 100. При числах Якоба выше 100 расхождение теории с экспериментальными данными увеличивается. При числе Якоба 792 расчетные значения диаметров пузырьков по своему порядку ниже экспериментальных. Данные по росту пузырьков во всем исследованном диапазоне чисел Рейнольдса обобщается выражением

$$D = 5\,N_{Ja}^{\frac{1}{2}}\sqrt{(\alpha t)}.$$

Совершенно очевидно, что современной теории роста пузырьков присущи серьезные недостатки и её необходимо переработать с учетом относительной роли динамических эффектов при больших числах Якоба.